Inelastic electron scattering in amorphous silicon nitride and aluminum oxide with multiple-scattering corrections

Peteris Livins, T. Aton,* and S. E. Schnatterly
Department of Physics, University of Virginia, Charlottesville, Virginia 22901
(Received 14 March 1988)

Electron-energy-loss measurements for an amorphous chemical-vapor-deposited silicon nitride film and evaporated sapphire in the broad energy range 1–200 eV are investigated. A method, not requiring the zero-loss peak, to remove the multiple scattering is discussed, applied, and the optical constants obtained. An Elliot-type model used with aluminum oxide gives a valence-exciton binding energy of 1.36±0.2 eV with a band gap of 9.8±0.2 eV. The unexpected strength of the nitrogen 2*s* transition is noted in silicon nitride.

I. INTRODUCTION

Inelastic electron scattering (IES) measurements provide information on electronic excitations over a wide energy range. Using such data to determine absolute values of the optical constants, however, is hindered by the multiple scattering effects. Although the recent access to synchrotron radiation has answered some of the needs for tunable sources, optical experiments are typically constrained to a limited spectral region. Also, optical-absorption measurements can easily be contaminated by pinholes in the films being studied, and multiple orders. Reflection experiments require clean and smooth surfaces. Removal of the multiple scattering in inelastic electron scattering is thus very desirable.

Techniques to remove multiple scattering in IES have previously been discussed and applied to the analysis of data. These techniques are either based on iterative deconvolution[1] or Fourier transform[2–4] methods. All such previous techniques rely on knowing the relative strength of the elastic peak in determining the strength of the multiple scattering. However, due to the large dynamic range needed in the signal between the elastic peak and the inelastically scattered data, any nonlinearity can introduce an error in the multiple scattering removal. This is particularly so in the Fourier transform methods, where even the large differences in the signal within the inelastically scattered data can produce difficulties when any small nonlinearity in the measurement apparatus exists. Often the simultaneous determination of the elastic peak and the inelastic data is not possible due to other technical reasons, and another approach is therefore necessary.

The multiple-scattering-removal technique that will be used here is based on a method developed by Fields,[5] where it was used to remove the double and triple scattering in the analysis of LiF data. It is an iterative method which, starting with energy convolutions of the data, estimates the multiple scattering and subtracts it, leaving an estimate of the single scattering spectrum. It will not require knowledge of the strength of the elastic peak and is therefore less susceptible to nonlinearities in the measuring apparatus. It is, however, necessary to know the oscillator strength in the f-sum rule for the transitions of concern, which can often be easily estimated to within 5%, or in principle calculated using atomic wave functions. Here we discuss the algorithm from a point of view which systematically allows its extension to any order of multiple scattering desired, and analyze IES measurements over a 200-eV range for amorphous films of chemical-vapor-deposited (CVD) silicon nitride and electron-beam-evaporated sapphire.

II. INELASTIC ELECTRON SCATTERING

In inelastic electron scattering an energetic (here 300 keV) electron passes through a thin film of the material being studied. The electron conveys a momentum transfer $\hbar\mathbf{q}$ and energy loss $\hbar\omega$. For relatively large incoming momentum $\hbar\mathbf{k}_0$ and scattering at small angles θ, the perpendicular and parallel components corresponding to the momentum transfer are given to excellent approximation by

$$|\mathbf{q}_\perp| = |\mathbf{k}_0|\,\theta\,, \tag{1}$$

$$|q_\parallel| = \frac{\omega}{v}\,, \tag{2}$$

where v is the incoming electron velocity. With highly energetic beams, the perpendicular component is far greater than the parallel component and thus the momentum transfer is dominated by the perpendicular component and essentially decoupled from the energy loss.

The aim of electron scattering is to obtain the differential cross section $d\Sigma/d\omega\, d^2\mathbf{q}_\perp$ for scattering at energy loss $\hbar\omega$, at some perpendicular momentum transfer $\hbar\mathbf{q}_\perp$, and per unit sample thickness, which is given by[6]

$$\frac{d\Sigma}{d\omega\, d^2\mathbf{q}_\perp} = \left[\frac{e}{\pi\hbar v}\right]^2 \frac{\hbar}{q^2}\,\mathrm{Im}\left[\frac{-1}{\epsilon(q,\omega)}\right], \tag{3}$$

where $\epsilon(\mathbf{q},\omega)$ is the complex dielectric constant. It is the loss function $\mathrm{Im}[-1/\epsilon(q,\omega)]$ in the long-wavelength limit ($\mathbf{q}=\mathbf{0}$) which provides the optical constants through a Kramers-Kronig analysis.

Since the total momentum transfer is not completely

decoupled from the energy loss, the factor $1/q^2$ does provide a weak energy dependence. We can write it as

$$\frac{1}{q^2}=\frac{1}{q_\perp^2+(\omega/v)^2} . \tag{4}$$

This factor, the kinematic factor, can provide a significant energy dependence for small q. At finite $q_\perp$ it might be thought that this dependence is negligible, but due to finite instrumental resolution, momentum transfers corresponding to small values of $q_\perp$ always contribute to some degree. Therefore the effective kinematic factor $K(\omega)$ is some weighted combination of kinematic factors for different $\mathbf{q}_\perp$. If one assumes that the loss function is q independent over a momentum resolution width, then a resolution weighted factor that gives the effective energy dependence can be calculated with

$$K(\omega)=\int \frac{1}{(\mathbf{q}_\perp-\mathbf{q}_\perp')^2+(\omega/v)^2} R(\mathbf{q}_\perp')d^2\mathbf{q}_\perp' , \tag{5}$$

where $R(\mathbf{q}_\perp)$ is the shape of the wave-vector resolution function. A knowledge of $K(\omega)$ is required if the loss function is to be determined from the data. We calculate this function numerically using a two-dimensional Gaussian for $R(\mathbf{q}_\perp)$. The instrumental resolutions [full width at half maximum (FWHM)] here are 0.06 Å^{-1} for the wave-vector resolution and 140 meV for the energy resolution.

The information gained through electron scattering is compared to optical data through the Kramers-Kronig dispersion relations,

$$\mathrm{Re}\left[\frac{1}{\epsilon(\mathbf{q},\omega)}\right]-1=\frac{1}{\pi}P\int_{-\infty}^{\infty}\mathrm{Im}\left[\frac{1}{\epsilon(\mathbf{q},\omega')}\right]\frac{1}{\omega'-\omega}d\omega' \tag{6}$$

and

$$\mathrm{Im}\left[\frac{1}{\epsilon(\mathbf{q},\omega)}\right]=-\frac{1}{\pi}P\int_{-\infty}^{\infty}\mathrm{Re}\left[\frac{1}{\epsilon(\mathbf{q},\omega')}\right]\frac{1}{\omega'-\omega}d\omega' . \tag{7}$$

Writing

$$\epsilon=1+\frac{1-1/\epsilon}{1/\epsilon} , \tag{8}$$

the real and imaginary parts of the dielectric constant are obtained with

$$\mathrm{Re}(\epsilon)=\epsilon_1=\frac{\mathrm{Re}(1/\epsilon)}{\mathrm{Re}(1/\epsilon)^2+\mathrm{Im}(1/\epsilon)^2} \tag{9}$$

and

$$\mathrm{Im}(\epsilon)=\epsilon_2=\frac{-\mathrm{Im}(1/\epsilon)}{\mathrm{Re}(1/\epsilon)^2+\mathrm{Im}(1/\epsilon)^2} . \tag{10}$$

A Kramers-Kronig analysis then provides the full dielectric constant, from which quantities such as the complex refractive index

$$n(\omega)=[\epsilon(\omega)]^{1/2} \tag{11}$$

or the absorption coefficient

$$\mu(\omega)=2\omega\,\mathrm{Im}\left[\frac{n(\omega)}{c}\right] \tag{12}$$

may be obtained.

An important relation to be used here is the f-sum rule,

$$\int_0^\infty \omega'\mathrm{Im}\left[\frac{-1}{\epsilon(\mathbf{q},\omega')}\right]d\omega'=\frac{2n_{\mathrm{eff}}e^2}{m} , \tag{13}$$

where n_{eff} is the density of electrons that contribute to the energy absorbing transitions and m is the electron mass. Of course, in integrating to infinity, all electrons in the solid should contribute, and more properly no qualification on what electron density to use should exist; it should be the total electron density. However, measuring data out to infinity asks too much of the experimentalist. Instead we note that the contribution to the energy absorption from a core state does not contribute significantly below that core's threshold. Typically such a threshold occurs high enough in energy that the response of the less bound contributing electrons is free-electron-like. Here, the data can be artificially extended with the free-electron response that a Drude model would predict, which is $1/\omega^3$, and n_{eff} would only include those electrons contributing up to the onset of the new core threshold.

Still, such a partitioning of the sum rule for certain groups of electrons is not rigorously correct. First of all, due to interactions, deep levels can still contribute to small energy losses in some higher-order virtual transition, although these effects are assumed to be quite negligible. More importantly, the effects of exclusion can significantly enhance the oscillator strengths from what one may estimate from simple counting of electrons.[7] For example, the simple counting of valence electrons in aluminum that contribute to the oscillator strength below the $2p$ core threshold gives three electrons per atom. The effects of exclusion enhance this number, and a self-consistent study of aluminum by Smith and Shiles,[8] using many sources of data, indicates that a more correct number of electrons per atom is 3.2. Since this number is usually not accurately known *a priori* (except possibly through calculation), the f-sum rule by itself may not accurately determine the scale of the loss function.

Another approach to scaling the data, which is used here, uses Eq. (6) and assumes that the electronic contribution to the loss function is relatively negligible and smooth as $\omega\to 0$, in which case we expect that

$$\mathrm{Re}\left[\frac{1}{\epsilon(\mathbf{q},0)}\right]-1=\frac{1}{\pi}\int_0^\infty \mathrm{Im}\left[\frac{1}{\epsilon(\mathbf{q},\omega')}\right]\frac{1}{\omega'}d\omega' , \tag{14}$$

where $\epsilon(\mathbf{q},0)$ corresponds to ϵ at optical frequencies. For $\epsilon(0)$ in insulators, we use the square of the index of refraction, or for metals we use infinity. Together the relations of Eqs. (13) and (14) help check results over a wide energy range, since the frequency factor emphasizes the

high-energy loss in the f-sum rule, and in Eq. (14) it emphasizes the low-energy loss.

III. MULTIPLE SCATTERING

The most problematic of the approximations made in the multiple scattering method used here is the assumption that the energy-loss function is weakly dependent on the wave vector. This of course is not the case for those materials where the plasmon loss or any other strong feature disperses rapidly with momentum transfer. It is this inability to deal with dispersion that unfortunately makes this technique less useful for many interesting materials that exhibit strong dispersion of narrow features. For those that do not, however, it provides an adequate solution to the multiple scattering dilemma.

With a thin film of some finite thickness t, the observed cross section $dI/d\omega\, d^2\mathbf{q}_\perp$ for scattering with energy loss $\hbar\omega$ and momentum transfer $\hbar\mathbf{q}_\perp$ includes multiple scattering events that may be expressed[5] by

$$\frac{dI(\omega,\mathbf{q}_\perp)}{d\omega\, d^2\mathbf{q}_\perp} \propto \sum_{n=1} \frac{t^n}{n!} \frac{d\Sigma_n(\omega,\mathbf{q}_\perp)}{d\omega d^2\mathbf{q}_\perp} , \tag{15}$$

where $(n>1)$

$$\frac{d\Sigma_n(\omega,\mathbf{q}_\perp)}{d\omega\, d^2\mathbf{q}_\perp} = \int\int_0^\omega \frac{d\Sigma_{n-1}(\omega',\mathbf{q}'_\perp)}{d\omega' d^2\mathbf{q}'_\perp} \frac{d\Sigma(\omega-\omega',\mathbf{q}_\perp-\mathbf{q}'_\perp)}{d\omega' d^2\mathbf{q}'_\perp} d\omega' d^2\mathbf{q}'_\perp \tag{16}$$

and

$$\frac{d\Sigma_1}{d\omega\, d^2\mathbf{q}_\perp} = \frac{d\Sigma}{d\omega d^2\mathbf{q}_\perp} . \tag{17}$$

The double scattering term is a convolution of the single scattering cross section, and higher-order terms are convolutions of the next lower term. These are weighted by a Poisson-like factor which depends on the sample thickness.

For the purposes of the wave-vector convolutions, the kinematic factor is taken to be energy independent. We use

$$F_1(\mathbf{q}_\perp) = \frac{1}{q_\perp^2+q_0^2} , \tag{18}$$

where q_0 is given by

$$q_0 = \frac{\omega_0}{v} , \tag{19}$$

and $\hbar\omega_0$ is the energy of the strongest feature in the spectrum. In this way, the error will be least where the correction is the greatest.

The need for such approximations arises due to the otherwise necessary three-dimensional (3D) integrations over frequency and momentum transfer $\hbar\mathbf{q}_\perp$. Data would be needed with many wave-vector values, and then would have to be properly interpolated. Furthermore, care would need to be observed that all data are taken with the same energy and momentum resolution. A uniform sample film is also necessary, since any beam drifts over many measurements might then penetrate different film thicknesses. With available computers, such repetitive 3D integrations are possibly quite feasible, but we have observed that the dispersion effects on multiple scattering are quite significant for sharp-featured data (plasmons in good metals, for instance) even at momentum transfers as low as $q_\perp = 0.1$ Å^{-1}. This would necessitate acquisition of data at lower momentum transfers, where the finite momentum resolution will significantly include the energy losses associated with Čerenkov radiation. For these reasons, we feel at present the approximations taken here are a practical compromise, since for many materials they will still be generally valid for momentum transfers near $q_\perp = 0.1$ Å^{-1}.

With the above approximations the cross section $d\Sigma/d\omega d^2\mathbf{q}_\perp$ is a separable product of the $\mathbf{q}_\perp$-dependent and ω-dependent factors $F_1(\mathbf{q}_\perp)$ and $\mathrm{Im}[-1/\epsilon(\omega)]$, respectively. Defining $S_1(\omega)=\mathrm{Im}[-1/\epsilon(\omega)]$, Eq. (15) becomes

$$\frac{dI}{d\,\omega d^2\mathbf{q}_\perp} = \xi\left[TF_1S_1 + \frac{T^2}{2}F_2S_2 + \frac{T^3}{6}F_3S_3 + \frac{T^4}{24}F_4S_4 + \cdots\right] , \tag{20}$$

where

$$T = \frac{t}{\hbar}\left[\frac{e}{\pi v}\right]^2 \tag{21}$$

and ξ is an arbitrary scale factor. S_n and F_n are given by $(n>1)$

$$S_n(\omega) = \int_0^\omega S_{n-1}(\omega-\omega')S_1(\omega')d\omega' , \tag{22}$$

$$F_n(\mathbf{q}_\perp) = \int F_{n-1}(\mathbf{q}_\perp-\mathbf{q}'_\perp)F_1(\mathbf{q}'_\perp)d^2\mathbf{q}' . \tag{23}$$

We can also write Eq. (20) as

$$f(\omega) = f_1 + a_2f_2 + a_3f_3 + a_4f_4 \cdots , \tag{24}$$

where $[f_0(\omega)=\delta(\omega)]$

$$f_n(\omega) = \int_0^\omega f_{n-1}(\omega-\omega')f_1(\omega')d\omega' = (\xi TF_1)^nS_n(\omega) \tag{25}$$

and f represents the measured count rate. The constants a_n are to be determined.

With the assumption that quadrupole- and higher-order multiple scattering is negligible, our goal is to obtain f_1 by removing the components a_2f_2 and a_3f_3. The algorithm will use the two equations

$$f_1 = f - \gamma g\circ g \tag{26}$$

and

$$g = f - \alpha\gamma g\circ g . \tag{27}$$

Here, $g\circ g$ indicates the self-convolution of the function $g(\omega)$,

$$g\circ g(\omega) = \int_0^\omega g(\omega-\omega')g(\omega')d\omega' , \tag{28}$$

The function $\gamma g \circ g$ represents the double and triple scattering. g itself is determined self-consistently from f by subtracting a fraction α of the multiple scattering. By leaving some double scattering within g, $g \circ g$ will include some triple scattering. That the correct strengths and shapes of the double and triple scattering are removed will of course depend on α, γ, and g.

At this point, we have four unknowns (α, γ, g, and f_1) and only two equations [Eqs. (26) and (27)], but as it will turn out, α is a constant that is determined by the physics. Thus starting with $g=f$, Eqs. (26) and (27) can be solved iteratively if some constraint on the resultant f_1 exists. Such a constraint is obtained with the f-sum rule [Eq. (13)] and the relation of Eq. (14), which require

$$\frac{\int_0^\infty d\omega\, \omega f_1(\omega)/K(\omega)}{\int_0^\infty d\omega\, f_1(\omega)/[\omega K(\omega)]} = \frac{2\pi n_{\text{eff}} e^2}{m[1-1/\epsilon(0)]} . \tag{29}$$

Here we have included the effective kinematic correction so that the proper shape for the loss function is used. After each iteration, the next value of γ is selected to satisfy Eq. (29), from which the following g is calculated [Eq. (27)], with which the resultant f_1 is constructed [Eq. (26)]. The process proceeds until some level of convergence is satisfied.

To obtain α, we will need to expand $g \circ g$ up to orders including f_3. Expanding Eq. (27) once gives

$$g \circ g = f \circ f - 2\alpha\gamma f \circ g \circ g + \alpha^2\gamma^2 g \circ g \circ g \circ g . \tag{30}$$

In including terms up to f_3 we only need to consider

$$g \circ g = f \circ f - 2\alpha\gamma f \circ f \circ f \cdots . \tag{31}$$

For reference, since we will eventually consider a quadrupole scattering, we expand several self-convolutions of f up to terms including f_4:

$$f \circ f = f_1 \circ f_1 + 2a_2 f_1 \circ f_2 + 2a_3 f_1 \circ f_3 + a_2^2 f_2 \circ f_2 + \cdots , \tag{32}$$

$$f \circ f \circ f = f_1 \circ f_1 \circ f_1 + 3a_2 f_1 \circ f_1 \circ f_2 + \cdots , \tag{33}$$

$$f \circ f \circ f \circ f = f_1 \circ f_1 \circ f_1 \circ f_1 + \cdots . \tag{34}$$

Now writing $\gamma g \circ g$ up to terms including f_3 gives

$$\gamma g \circ g = \gamma f_2 + (2\gamma a_2 - 2\alpha\gamma^2) f_3 + \cdots . \tag{35}$$

In equating corresponding terms with Eqs. (24) and (26), we obtain

$$a_2 = \gamma , \tag{36}$$

$$a_3 = 2\gamma a_2 - 2\alpha\gamma^2 = 2\gamma^2(1-\alpha) . \tag{37}$$

Here we have related α and γ for arbitrary a_n. However, the constants a_n, relating the relative strengths of the different multiple scattering contributions, are not arbitrary; their relative strengths are determined with Eq. (20). For a given overall scale factor ξ, once a_2 is known so are all the higher-order terms a_n. That this is the case can be seen by considering the ratios of corresponding terms from Eqs. (20) and (24), which for the first two terms give

$$\frac{a_2 f_2}{f_1} = \frac{TF_2S_2}{2F_1S_1} . \tag{38}$$

With the help of Eq. (25) we arrive at

$$a_2 = \frac{F_2}{2\xi F_1^2} . \tag{39}$$

Similarly,

$$a_3 = \frac{F_3}{6\xi^2 F_1^3} , \tag{40}$$

$$a_4 = \frac{F_4}{24\xi^3 F_1^4} , \tag{41}$$

and so on.

In particular, the ratios a_n/a_2^{n-1} will be constants independent of the thickness or scale factor. For instance,

$$\frac{a_3}{a_2^2} = \frac{2F_1F_3}{3F_2^2} , \tag{42}$$

$$\frac{a_4}{a_2^3} = \frac{F_1^2F_4}{3F_2^3} . \tag{43}$$

Thus, the above system of equations [Eqs. (36) and (37)] gives

$$\frac{a_3}{a_2^2} = 2(1-\alpha) = \frac{2F_1F_3}{3F_2^2} , \tag{44}$$

or

$$\alpha = 1 - \frac{F_1F_3}{3F_2^2} . \tag{45}$$

Therefore α is indeed a constant independent of the thickness or the scale. The functions F_n are evaluated at the value $\mathbf{q}_\perp$ at which the data were taken. Numerically obtained values for α at $q_\perp \approx 0.1$ Å^{-1} are typically near $\frac{3}{4}$. The self-consistent sample thickness t is obtained by combining

$$\gamma = a_2 = \frac{F_2}{2\xi F_1^2} \tag{46}$$

with

$$f_1 = \xi T F_1 S_1 , \tag{47}$$

giving

$$t = \hbar \left[\frac{\pi v}{e}\right]^2 \frac{2\gamma F_1}{F_2} \left[\frac{f_1}{S_1}\right] , \tag{48}$$

where γ and the ratio f_1/S_1 are outputs of the algorithm.

The above algorithm to remove double and triple scattering works precisely because the parameter α is a known constant, thus Eqs. (26) and (27) can be solved iteratively. Extending such a procedure to higher multiple orders then requires that any additional parameters

can also be determined *a priori*.

Although tedious, one can correct to any necessary $n+1$ multiple scattering order by considering equations

$$f_1 = f - \gamma g \circ g - \gamma^2 g \circ g \circ g - \cdots - \gamma^{n-1}(g\circ)^n \quad (49)$$

and

$$g = f - \alpha_1 \gamma g \circ g - \alpha_2 \gamma^2 g \circ g \circ g - \cdots - \alpha_{n-1}\gamma^{n-1}(g\circ)^n , \quad (50)$$

where $(g\circ)^n$ signifies the $(n-1)$th self-convolution of g. Besides the added energy convolution, each added order requires calculating another convolution over $\mathbf{q}_\perp$ for F_n. Fortunately, the assumption of little dispersion in the loss function is less troubling in higher orders, since smaller and smaller values of $q_\perp$ are strongly weighted in higher multiple scattering.

For the case $n=3$ (inclusion of quadrupole scattering) Eq. (50) can be expanded once, and a similar analysis as before yields the system of equations

$$a_2 = \gamma , \quad (51)$$

$$a_3 = \gamma^2(3-2\alpha_1) , \quad (52)$$

$$a_4 = \gamma^3(5\alpha_1^2 - 12\alpha_1 + 2\alpha_2 + 10) , \quad (53)$$

giving

$$\alpha_1 = \frac{3}{2} - \frac{F_1 F_3}{3F_2^2} \quad (54)$$

and

$$\alpha_2 = \frac{F_1^2 F_4}{6F_2^3} + \frac{F_1 F_3}{3F_2^2} - \frac{5F_1 F_3^3}{18F_2^4} - \frac{7}{8} . \quad (55)$$

However, it will be assumed that the quadrupole scattering is negligible, and only the double and triple scattering will be removed in the data analysis here.

In this approach the strength of the multiple scattering hinges on the ratio on the right-hand side of Eq. (29), which we will refer to as the ratio parameter. This number depends on n_{eff}, which, as pointed out, is not known accurately beforehand. Furthermore, this ratio parameter also depends on the sample density and its infrared refractive index, the values of which might not be well documented for the phase of the particular thin film being studied, although in principle they can be measured. This is often the case for amorphous films. However, even when these parameters are not accurately known, the ratio parameter is still known to within some plausible range, and can then be varied slightly to produce the most "reasonable" result. Unfortunately, this uncertainty introduces some subjectivity in the data analysis. This leeway might further be reduced by correlation with data from other techniques.

These uncertainties can be completely avoided if the sample thickness is known. The ratio parameter is then varied until the self-consistent thickness is consistent with the known thickness. This then also provides the oscillator strength if the density and refractive index are known. The usefulness of knowing the sample thickness cannot be understated.

IV. ALUMINUM OXIDE

As an example of this procedure, we first consider the amorphous aluminum oxide. The sample was produced with electron beam evaporation of sapphire (crystalline aluminum oxide), where a crystal thickness monitor measured a film thickness of 300 Å. The sample is therefore fairly thin and should exhibit weak multiple scattering. In addition, the thickness is known, so that the reliability of the multiple scattering subtraction is enhanced. The substrate was a salt crystal, from which the film was floated off and picked up on a 50-mm copper mesh.

The density of amorphous anodized aluminum oxide has been quoted by Swanson[9] as 2.8 g/cm^3 as opposed to 3.96 (Ref. 10) for sapphire. The refractive index for electron-beam-evaporated aluminum oxide has been measured by Cox[11] to be 1.7. In the application of the multiple scattering algorithm we have set the density at 3.0 g/cm^3 and $\epsilon(0)=2.9$, leaving the electron number per molecular unit (Al_2O_3) to vary the ratio parameter. A self-consistent thickness of 305 Å is obtained with 43 electrons per molecular unit. A naive counting of electrons contributing (aluminum $2s,2p,3s,3p$ and oxygen $2,2p$) gives 40 per molecular unit. As expected the oscillator strength is enhanced, although the meaning of any of the parameter values must be taken in light of the other numbers.

The Al_2O_3 data ($q_\perp = 0.11$ Å^{-1}) with the multiple scattering correction and resultant loss function appear in Fig. 1. Figure 2 gives ϵ_1 and ϵ_2 over various energy

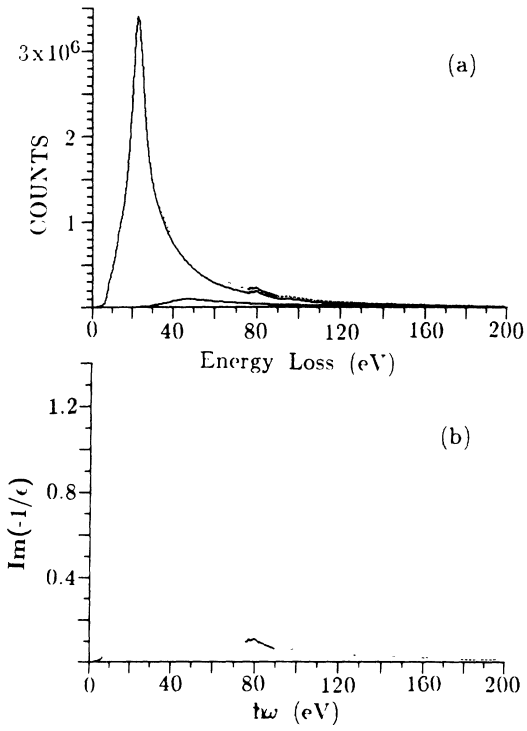

FIG. 1. (a) Electron scattering data for evaporated sapphire (dots) with the multiple scattering corrected result (upper solid line) and the subtracted strength (lower solid line). (b) Determined loss function for evaporated sapphire.

regions. The loss function is the multiple scattering corrected data, which has been modified by the kinematic correction and normalized to satisfy Eq. (14).

The aluminum oxide exhibits a loss maximum at 22.7±0.05 eV. The signature of a plasmon is a zero crossing for ϵ_1, with a small value for ϵ_2. Lacking a better description, this peak might be viewed as a poor plasmon, although as can be seen from Fig. 2, ϵ_1 almost, but does not cross zero at an energy near the peak of the data. At ≈77 eV the aluminum $2p$ core threshold exhibits a strong core exciton. Thresholds for s core transitions are usually very weak. Apparently the symmetry of the s core and a conduction state is such that the matrix elements are relatively small compared to the p cores, at least near threshold. Nevertheless, a weak feature appears near 125 eV in aluminum oxide and also near 155 eV in silicon nitride, close to the expected s core thresholds. In both aluminum oxide and silicon nitride, data extend approximately 100 eV above these thresholds so that the response at these energies should be free-electron-like.

Two features (Fig. 3) near 9 and 14 eV are observed, and a third has also been mentioned by Swanson[9] a 17.7 eV for sapphire. That the feature near 9 V might correspond to a valence exciton is here investigated by fitting an Elliott[12]-type model in the region 5–11 eV. The fitting

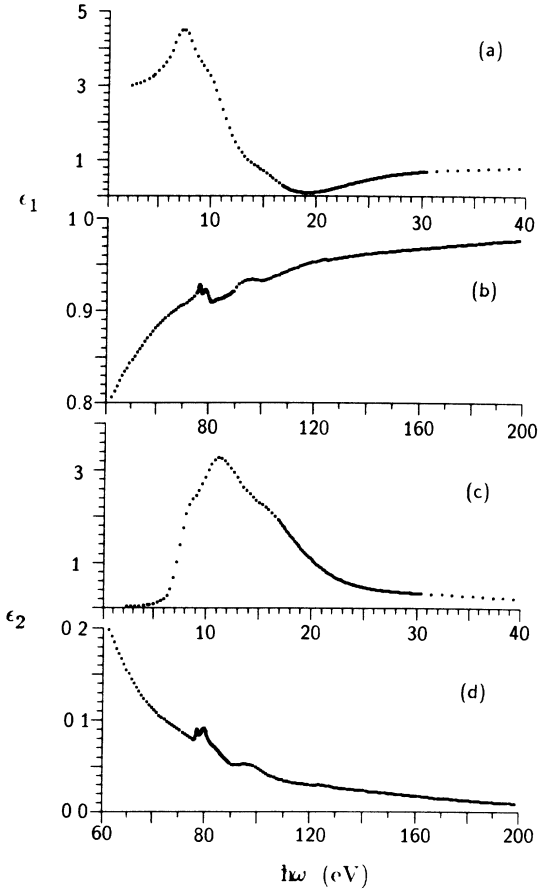

FIG. 2. Real [(a), (b)] and imaginary [(c), (d)] parts of the dielectric constants for evaporated sapphire.

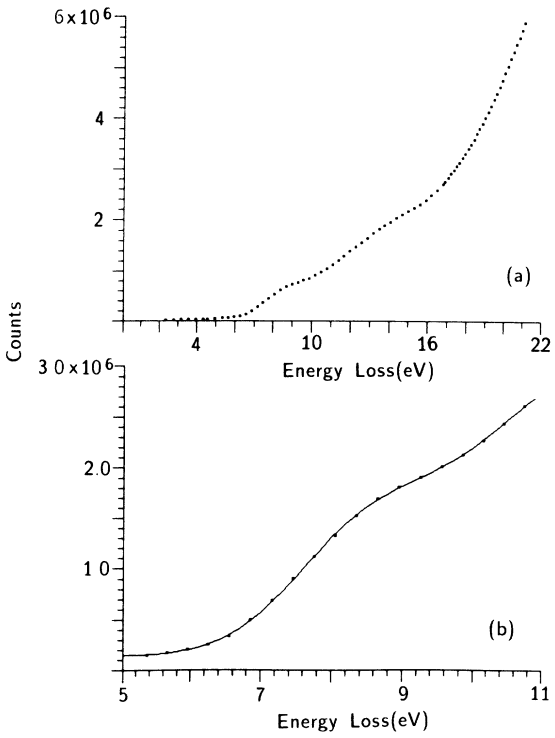

FIG. 3. (a) Low-energy loss for evaporated sapphire and (b) an Elliot-like model fit to excitonic feature.

function is the Gaussian convolution of the function $\Theta(x-E_c)C[ax+1]+b$ together with the Gaussian convolved hydrogenic series $D\sum_n[1/n^3\exp[-(x-E_n)^2/2\sigma^2]$. E_c is the continuum threshold, and $E_n=E_c-E_b/n^2$ where E_b is the $1s$ binding energy. C, D, σ, a, and b are arbitrary constants and $\Theta(x)$ is a step function at the origin with unit height. Thus we use seven fitting parameters. This fitting function is

$$f(x)=C\left\{\frac{ax+1}{2}\left[\operatorname{erf}\left[\frac{x-E_c}{\sigma\sqrt{2}}\right]+1\right]+\frac{a\sigma}{\sqrt{2\pi}}\exp\left[-\frac{(x-E_c)^2}{2\sigma^2}\right]\right\}+b$$
$$+D\sum_n^{\infty}(1/n^3)\exp[-(x-E_n)^2/2\sigma^2]\,. \quad (56)$$

The least-squares fit appears in Fig. 3. The resultant parameters give a $1s$ exciton binding energy of 1.36 eV and a continuum threshold of 9.80 eV; σ is 1.0 eV. These values can be compared to a binding energy of 0.6 eV and band gap of 8.7 eV, also derived from electron scattering.[13] The latter parameters were determined through a fitted model dielectric function, which however did not include the effects of the electron-hole interaction above the continuum threshold. Such procedure, with smoothly increasing strength above threshold, would naturally fit with a smaller band gap and binding energy. A true Elliot model assumes the validity of the Wannier-Mott limit, which we have not attempted to demonstrate, and with which the rather large binding energy would be at

odds. Instead, with C and D as independent parameters, the model is viewed here simply as a model that includes effects of the electron-hole interaction on the continuum levels in order to extract a band gap and exciton binding energy.

Another interpretation of the low-energy data in aluminum oxide is an excitonic resonance above the continuum threshold, as has been discussed regarding SiO_2.[14] In such a case, the matrix elements at threshold are small, removing the effect of a step function, and the feature observed is considered to lie within the continuum above threshold. To explore such a possibility, we replace the step-function term $\Theta(x-E_c)C[ax+1]$ with $\Theta(x-E_c)C[x-E_c]$, and the excitonic series with a single Gaussian with negative binding energy. Thus we use a threshold that turns on linearly from zero at E_c, with a symmetric resonance added somewhere above the continuum threshold. The corresponding Gaussian broadened expression is obtained from Eq. (56) by replacing the coefficient $ax+1$ by $x-E_c$ and the coefficient $a\sigma$ by σ. The resulting fit gives a continuum threshold at 7.03 eV and the resonance centered at 8.28 eV; σ is 0.94 eV. Both fits work equally well, and thus the data are not decisive in choosing either point of view suggested here.

V. SILICON NITRIDE

The silicon nitride sample is a thin film produced through chemical vapor deposition. The film was grown on a silicon substrate which was subsequently removed, thus producing a free-standing silicon nitride film, however with unknown thickness.

Electron scattering data ($q_\perp = 0.10$ Å^{-1}) and the multiple scattering corrected results for silicon nitride appear in Fig. 4. The plasma resonance is the main feature at 22.5 ± 0.1 eV. That this feature does indeed represent a collective loss is apparent from the Kramers-Kronig analysis (Fig. 5), which shows a true zero crossing for ϵ_1. The feature in the loss function 45 eV, as we will argue, is not a failure of the multiple scattering method, but strength contributed due to the $2s$ nitrogen transition. Near 103 eV is a sharp threshold representing the onest of the silicon $2p$ core electrons.

Since the thickness of the silicon nitride sample was not known, the determination of the multiple scattering correction requires some other arguments for the final choice of the ratio parameter. For valence and $n=2$ core states, the simple counting of electrons contributing to n_{eff} for the stoichiometry of silicon nitride gives 56 electrons for the unit Si_3N_4. However, the mass densities of CVD films for silicon nitride vary (2.6–3.2 g/cm^3) in the literature,[15,16] crystalline films naturally being denser than amorphous films, and in the amorphous case being sensitive to the deposition conditions. The film density in this case was not known; we will assume it to be 3.0 g/cm^3, and use 1.99 for the refractive index.[17,18] Since the number of electrons and the density will enter in n_{eff} as a product, the leeway in the multiple scattering removal will involve varying the number of electrons from the number 56.

ϵ_2 will depend sensitively on the multiple scattering re-

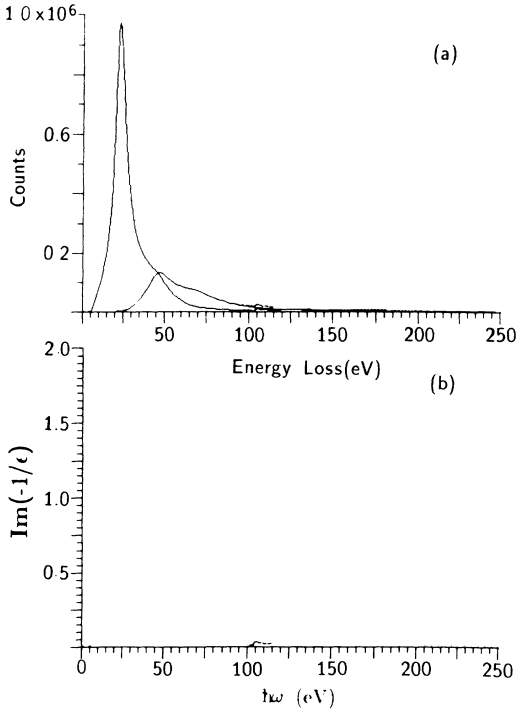

FIG. 4. (a) Electron scattering data for amorphous silicon nitride (dots) with the multiple scattering corrected result (upper solid line) and the subtracted strength (lower solid line). (b) Determined loss function for amorphous silicon nitride.

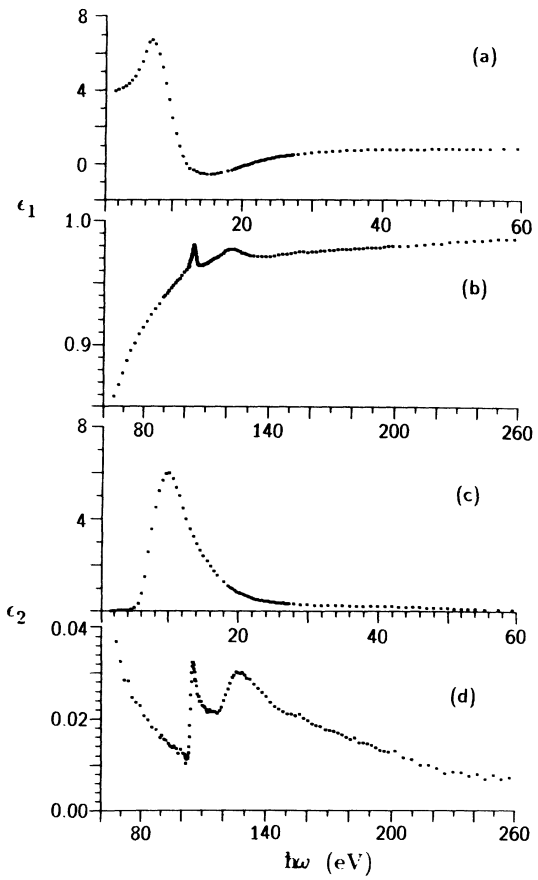

FIG. 5. Real [(a), (b)] and imaginary [(c), (d)] parts of the dielectric constants for amorphous silicon nitride.

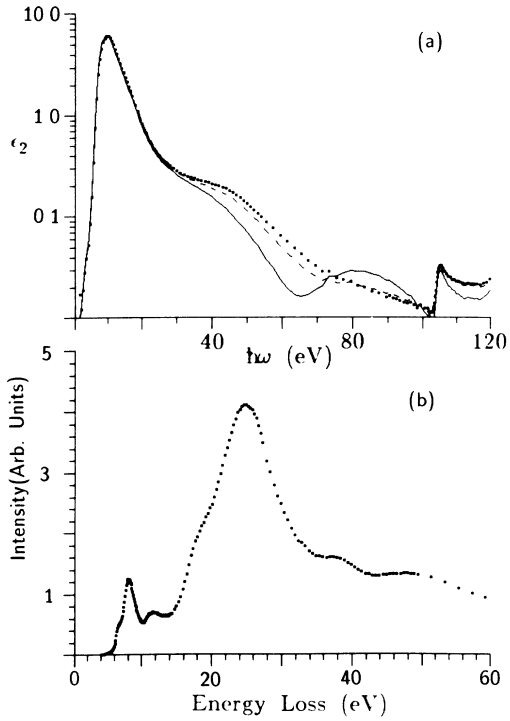

FIG. 6. (a) Several determinations of ϵ_2 for n_{eff} corresponding to 56 (solid), 61 (dashed), and 65 (dots) electrons per Si_3N_4. (b) Electron scattering data for boron nitride (with no correction for multiple scattering).

moval in the region of the plasmon triple scattering (≈ 67 eV). Here the signal is relatively small compared to the plasma loss, so removal of the triple plasma loss can be a significant portion of the signal. Removal of too much or too little will produce unphysical results for ϵ_2. Figure 6 shows resultant ϵ_2 for various electron numbers per Si_3N_4 unit. Having chosen the density at 3.0 g/cm^3 we shall expect that the electron number be somewhat greater than 56.

Although subjective, it appears that the most reasonable results occur when the electron number is chosen to be 65. It is reassuring that in varying the electron number the value of ϵ_2 changes significantly only in the region 50–100 eV. In particular, the strength of the absorption edge is not modified. This allows an absolute rather than a relative determination of the absorption coefficient, which is still a rare event in the literature.

That the multiple scattering removal left strength in the region near 45 eV was at first troubling, since it occurred near double scattering of the plasmon. The ratio parameter can be chosen so that the high-energy region of the plasmon appears smooth and symmetrical, but then the strength near 50 eV becomes negative. It was expected that the nitrogen 2s transition would be very weak, and could not account for the strength observed. Furthermore the proximity of the feature at twice the plasmon energy cast doubt on the multiple scattering removal, although such a gross failure could not be understood.

In the analysis where the resulting ϵ_2 was obtained for different ratio parameters, it is clear that the feature near 45 eV is not an artifact of the multiple scattering removal. This suggests that the 2s nitrogen transition is actually contributing significantly, and with a strength stronger than most 2s core transitions. An independent verification of the strength of this transition also appears in data for boron nitride,[19] where the double plasmon loss is further separated from the nitrogen 2s core feature. In boron nitride (Fig. 6), the feature is distinct from the plasmon double scattering, and uncharacteristically strong for a 2s core transition. This fact is reassuring. With it, all the pieces fit together in the interpretation that our multiple scattering removal is indeed correct. It points out the importance of a multiple-scattering-removal algorithm; without such a method, the contribution of the 2s nitrogen core transition in silicon nitride could go unnoticed.

As in the case of aluminum oxide, a feature appears near the conduction-band threshold region in silicon nitride, although much weaker. A similar fitting analysis was done to investigate it. Again, both the models for a bound state or an excitonic resonance fit equally well. Parameters for the bound state give the continuum threshold at 9.45 eV with a 1s binding energy of 1.53 eV, and $\sigma = 1.31$ eV. For an excitonic resonance, the continuum threshold sits at 6.37 eV with the resonance centered at 7.55 eV, and $\sigma = 1.17$ eV. Most reported band gaps for silicon nitride do not exceed 5.3 eV.[17,20–22] However, these approaches define the band gap as the onset of absorption without any regard to final-state interactions. Band-structure calculations[23] place the band gap near 6 eV. Also, the bound-state model, with the large binding energy together with such a weak feature, would then seem inconsistent with the bound-state view. Thus it seems more likely that the low-energy spectra for silicon nitride reflect either an excitonic resonance or simply a structure in the joint density of states.

ACKNOWLEDGMENTS

We would like to thank other collaborators who are or have been involved during this research, P. Bruhwiler, R. Carson, D. Husk, J. Nithianandam, C. Tarrio, and S. Velasquez; also Dr. A. A. Cafolla and Dr. A. Mansour for helpful suggestions and discussions throughout the course of this work. We also thank IBM for providing the silicon nitride film. This research was supported in part by the National Science Foundation (Grant No. DMR 85-15684).

*Present address: Texas Instruments, Dallas, TX 75265.

[1] C. Wehenkel, J. Phys. (Paris) **36**, 199 (1975).
[2] D. L. Misell and A. F. Jones, J. Phys. A **2**, 540 (1969).
[3] P. Bateson and J. Silcox, Phys. Rev. B **27**, 5224 (1983).
[4] R. F. Egerton, B. G. Williams, and T. G. Sparrow, Proc. R. Soc. London Ser. A **398**, 395 (1985).
[5] J. Fields, Ph.D. thesis, Princeton University, Princeton, NJ, 1975.

[6]S. E. Schnatterly, *Solid State Physics* (Academic, New York, 1979), Vol. 34, p. 275.
[7]F. Wooten, *Optical Properties of Solids* (Academic, New York, 1972), p. 75.
[8]D. Y. Smith and E. Shiles, Phys. Rev. B **17**, 4689 (1978).
[9]N. Swanson, Phys. Rev. **165**, 1067 (1968).
[10]*CRC Handbook of Chemistry and Physics,* edited by R. C. Weast (Chemical Rubber Co., Cleveland, 1985).
[11]J. T. Cox, J. Phys. (Paris) **25**, 250 (1964).
[12]R. J. Elliott, Phys. Rev. **108**, 1384 (1957).
[13]W. Tews and R. Zimmermann, Phys. Status Solidi B **110**, 479 (1982).
[14]R. B. Laughlin, Phys. Rev. B **22**, 3021 (1980).
[15]K. Niihara, and T. Hirai, J. Mater. Sci. **11**, 604 (1976).
[16]E. V. Shitova, A. Yasneva, and N. A. Genkina, Opt. Spektrosk. **43**, 244 (1977) [Opt. Spectrosc. (USSR) **43**, 140 (1977)].
[17]J. Bauer, Phys. Status Solidi **39**, 411 (1977).
[18]J. M. Andrews, B. G. Jackson, and W. J. Polito, J. Appl. Phys. **51**, 495 (1980).
[19]C. Tarrio (unpublished).
[20]D. M. Brown *et al.*, J. Electrochem. Soc. **115**, 311 (1969).
[21]I. I. Zhukova, V. A. Fomichev, A. S. Vinogradov, and T. M. Zimkina, Fiz. Tverd. Tela (Leningrad) **10**, 1383 (1968) [Sov. Phys.—Solid State **10**, 1097 (1968)].
[22]A. M. Goodman, Appl. Phys. Lett. **13**, 275 (1968).
[23]S. Ren and W. Y. Ching, Phys. Rev. B **23**, 5454 (1981).